Interplay of spin and charge order in the electron-doped cuprates

David Riegler [1,2,*] Jannis Seufert [1] Eduardo H. da Silva Neto [3,4,5,6] Peter Wölfle [2,7]
Ronny Thomale [1] and Michael Klett [1,†]

[1]*Institute for Theoretical Physics, University of Wuerzburg, D-97074 Wuerzburg, Germany*
[2]*Institute for Theory of Condensed Matter, Karlsruhe Institute of Technology, D-76128 Karlsruhe, Germany*
[3]*Department of Physics, Yale University, New Haven, Connecticut 06511, USA*
[4]*Energy Sciences Institute, Yale University, West Haven, Connecticut 06516, USA*
[5]*Department of Applied Physics, Yale University, New Haven, Connecticut 06511, USA*
[6]*Department of Physics, University of California, Davis, California 95616, USA*
[7]*Institute for Quantum Materials and Technologies, Karlsruhe Institute of Technology, D-76021 Karlsruhe, Germany*

(Received 15 June 2023; revised 19 October 2023; accepted 20 October 2023; published 21 November 2023)

We study magnetic and charge order in the electron-doped high-T_c cuprates based on the one-band Hubbard model with onsite U and nearest-neighbor V interactions. To investigate the interplay between the orders, we employ the Kotliar-Ruckenstein slave-boson method and analyze fluctuations descending from an antiferromagnetic parent state. Our analysis reveals incommensurate charge order whose ordering vector matches the doping dependence of resonant inelastic x-ray scattering (RIXS) measurements in $Nd_{2-x}Ce_xCuO_4$ (NCCO). From our calculations of paramagnon dispersion as well as dynamical charge and spin structure factors, we reproduce the characteristic features of the RIXS signal.

DOI: 10.1103/PhysRevB.108.195141

Introduction. In recent years, charge order (CO) has been found to complement spin order (SO) as an integral part of the low-energy physics of cuprate superconductors [1–15]. Through various experiments showing either the suppression of CO with the onset of superconductivity or the enhancement of CO with a suppression of it, there is accumulating evidence on their competing character [1,4,7,15]. Still, dynamic fluctuations of CO type pervade the entire cuprate phase diagram [13,14,16], suggesting their quintessential role in cuprate phenomenology. The intertwining of CO and SO features important qualitative differences in electron- and hole-doped cuprates [2]: The commensurate antiferromagnetic (AFM) phase extends to larger dopings in electron-doped cuprates whereas it becomes incommensurate in various hole-doped compounds, with significant impact on the nature of CO [1,10,17]. Furthermore, phase separation (PS) [18], i.e., an inhomogeneous mixture of insulating magnetic and metallic domains, is well established for hole-doping but is assumed to be absent in electron-doped cuprates [2].

The one-band Hubbard model in two dimensions (2D) with onsite repulsion U has been established as a minimal model to theoretically describe cuprate systems, and is assumed to also model finite hole- and electron-doping. Accounting for the dissimilarity of hole-doped and electron-doped cuprates, particle-hole asymmetry is already implied at the single-particle level by next-to-nearest-neighbor (NNN) hopping t' [19–22]. *Ab initio* calculations further imply a non-negligible nearest-neighbor (NN) repulsion V [21,23], which is suggested to be relevant in capturing the phenomenology of static and dynamic charge order in hole-doped cuprates [24–26]. In absence of an exact solution, a variety of different approximations and computational methods have been developed for the Hubbard model [27]. Resolving the intertwined nature of SO and CO poses a particular numerical challenge, as it implies the necessity of addressing incommensurate order and dynamical correlation functions.

In this article, we develop a theory of intertwined charge and spin order for electron-doped cuprates. We adopt the Kotliar-Ruckenstein slave-boson (KRSB) ansatz [28] which we have recently generalized to address a magnetic mean field and dynamic fluctuations around the symmetry-broken state [29]. We find that even moderate V has a decisive impact on the electron-doped regime by removing its propensity to phase-separation. From a commensurate AFM parent state, we calculate the dynamical spin and charge susceptibility as a function of electron-doping. We discover a strong interdependence between charge fluctuations and the longitudinal spin channel. Enabled by KRSB to calculate the doping dependence of the ordering vectors, paramagnons, plasmons, and the dynamical spin and charge structure factors, we obtain good agreement with experimental findings in $Nd_{2-x}Ce_xCuO_4$ (NCCO) [9,11,30,31].

Model and method. We employ the extended one-band t-t' U-V Hubbard model on the 2D square lattice with onsite repulsion U and NN interaction V defined by

$$H = -\sum_{\sigma=\uparrow,\downarrow}\left(t\sum_{\langle i,j\rangle_1} c^\dagger_{i,\sigma}c_{j,\sigma} + t'\sum_{\langle i,j\rangle_2} c^\dagger_{i,\sigma}c_{j,\sigma} + \text{H.c.}\right) - \mu_0\sum_i n_i + U\sum_i c^\dagger_{i,\uparrow}c_{i,\uparrow}c^\dagger_{i,\downarrow}c_{i,\downarrow} + V\sum_{\langle ij\rangle_1} n_i n_j, \quad (1)$$

*david.riegler@kit.edu
†michael.klett@uni-wuerzburg.de

where the operator $c^\dagger_{i,\sigma}$ creates an electron with spin $\sigma = \{\uparrow, \downarrow\}$ at site i, and $n_i = \sum_\sigma c^\dagger_{i,\sigma} c_{i,\sigma}$. Moreover, $\langle i, j\rangle_n$ denotes a nth nearest-neighbor pair, and μ_0 is the chemical potential. We employ $t'/t = -0.2$ throughout the paper, which is a generic choice to approximate a large family of cuprate materials [20–22] and measure energy in units of t.

Slave-boson mean-field approximation. We apply the spin-rotation invariant Kotliar-Ruckenstein slave-boson (SRIKR-SB) representation [28,32], whereby we introduce the bosonic fields e_i, d_i, $p_{0,i}$, and $\boldsymbol{p}_i$ which label empty, doubly, and singly occupied states respectively, as well as a set of auxiliary fermionic fields $\boldsymbol{f}_i$ and Lagrange multiplier fields α_i, $\beta_{0,i}$, $\boldsymbol{\beta}_i$ to recover the physical subspace via constraints. We then determine the ground state within a static mean-field (MF) ansatz, where bosonic fields that couple to charge degrees of freedom, i.e., $\psi_{\mu,i} \in \{\alpha_i, e_i, d_i, p_{0,i}, \beta_{0,i}\}$ are approximated to be spatially uniform, whereas the spin degrees of freedom, i.e., $\psi_{\mu,i} \in \{\boldsymbol{p}_i, \boldsymbol{\beta}_i\}$ are constrained to a spin spiral with ordering vector $\boldsymbol{Q}_{\rm SO}$. The resulting MF expectation values of the charge and spin operator are given by $n_i \to \langle n\rangle = 1 + d^2 - e^2$ and $\boldsymbol{S}_i \to \langle \boldsymbol{S}_i\rangle = p_0|\boldsymbol{p}|[\cos(\boldsymbol{Q}_{\rm SO}\boldsymbol{r}_i), \sin(\boldsymbol{Q}_{\rm SO}\boldsymbol{r}_i), 0]$, where $|\boldsymbol{p}| \neq 0$ implicates magnetic order. The MF ground state is thereby determined by the saddle point of the free energy, where the constraints are enforced on average. As we derive in the Supplemental Material (SM) [33], the addition of V shifts the chemical potential μ_0 and Lagrange-multiplier β_0

$$\mu_0 = \mu_0|_{V=0} + 4Vn, \quad \beta_0 = \beta_0|_{V=0} + 4Vn, \tag{2}$$

whereas all other MF variables are agnostic to V. The MF band structure remains unchanged since it only depends on $\mu_0 - \beta_0$ [34–36].

Gaussian fluctuations. Beyond mean field, we consider fluctuations around the saddle point through expanding the action $\mathcal{S}$ up to second order in bosonic fields, i.e., calculating

$$\mathcal{M}^{ab}_{\mu\nu}(\boldsymbol{q}, \mathrm{i}\omega_n) = \frac{1}{2}\frac{\delta^2\mathcal{S}(\psi)}{\delta\psi_{\mu,-\boldsymbol{q}-a\boldsymbol{Q}_{\rm SO},-\mathrm{i}\omega_n}\,\delta\psi_{\nu,\boldsymbol{q}+b\boldsymbol{Q}_{\rm SO},\mathrm{i}\omega_n}}. \tag{3}$$

The established formalism [37,38] has recently been extended to encompass symmetry-broken states [29], which we apply to calculate susceptibilities descending from AFM mean-field saddle points, i.e., $\boldsymbol{Q}_{\rm SO} = (\pi, \pi)$ with the Umklapp momenta $a, b \in \{0, 1\}$. The spin susceptibility is composed of the longitudinal part parallel to the staggered MF magnetization $\chi^l_s(\boldsymbol{q}, \omega) = \langle \delta S^x_{\boldsymbol{q},\omega}\, \delta S^x_{-\boldsymbol{q},-\omega}\rangle$ that couples to the charge susceptibility $\chi_c(\boldsymbol{q}, \omega) = \langle \delta n_{\boldsymbol{q},\omega}\, \delta n_{-\boldsymbol{q},-\omega}\rangle$ and a perpendicular, i.e., transversal part $\chi^t_s(\boldsymbol{q}, \omega) = \langle \delta S^y_{\boldsymbol{q},\omega}\, \delta S^y_{-\boldsymbol{q},-\omega}\rangle = \langle \delta S^z_{\boldsymbol{q},\omega}\, \delta S^z_{-\boldsymbol{q},-\omega}\rangle$ that is decoupled due to a block diagonality in $\mathcal{M}^{ab}_{\mu\nu}$. Notably, we show in the SM along with a recap of the SB theory that the newly implemented interaction V generates additional contributions for the charge fields e, d_1, d_2 in the bosonic part of the fluctuation matrix [33].

Mean-field analysis. In agreement with previous SB studies of the Hubbard model [34–36,39,40], we determine incommensurate spiral magnetism for hole doping [$\boldsymbol{Q}_{\rm SO}/2\pi = (\frac{1}{2}, \frac{1}{2} - \delta)$ along with $\boldsymbol{Q}_{\rm SO}/2\pi = (\frac{1}{2} - \delta, \frac{1}{2} - \delta)$] and an extended commensurate AFM domain for electron doping [$\boldsymbol{Q}_{\rm SO}/2\pi = (\frac{1}{2}, \frac{1}{2})$], which is further supported by other theoretical methods [41,42]. Moreover, the incommensurability δ is proportional to the doping x [34,40], and in fact in agreement with the Yamada relation $\delta \approx x$ [43] known from La-based cuprate families [17,44,45]. The doped magnetic MF ground state, however, is known to become unstable beyond a critical interaction [29,40,46,47], which is signaled by a negative compressibility $\kappa_T \propto \partial n/\partial\mu_0 < 0$. Thereby, $\kappa_T^{-1} = \chi_c^{-1}(\boldsymbol{q} = 0) = 0$ describes the tipping point where the MF ground state is no longer stable against charge fluctuations. We find that this is avoided by the formation of two coexisting, individually stable condensates with different fillings and the same chemical potential, i.e., phase separation (PS): The undoped, strongly magnetized and insulating AFM mixes with a metallic state carrying the doped holes or electrons with a lower net magnetization. While a weakly-interacting system tends to delocalize its charge carriers uniformly to gain kinetic energy, the potential energy scale set by the strong effective AFM Heisenberg exchange of the half-filled Hubbard model becomes dominant at low dopings. This is why the PS scenario is favored over a uniform AFM, as it partially recovers the pristine crystal [29,35,36]. For hole doping, we associate PS obtained from our MF theory with the much discussed stripe phases [10,18] and find the ground-state energies to be comparable to those of an SB cluster study with large unit cells [48], compare Fig. 8.14(b) in Ref. [35]. Repulsive V drastically reduces phase-separated domains, which is due to the chemical potential shift described by Eq. (2) and can intuitively be understood by the thereby effectively reduced AFM Heisenberg exchange. In particular, PS is found to be comparably resilient for hole doping, whereas already rather small values of V eliminate this ordering tendency for electron doping as further elaborated in the SM [33]. In agreement with this emergent particle-hole asymmetry in our theory, PS has so far only been observed in hole-doped cuprate families [2,49–52]. Moreover, for NCCO, precise measurements of core-level photo-emission spectra have shown that $\mu_0(n)$ is a monotonous function, i.e., that PS should be absent [52].

Fluctuation analysis. Motivated by the above established fragility of PS under electron doping, we are particularly interested in other types of charge inhomogeneities emerging from the associated commensurate AFM domain and apply the fluctuation formalism for a more in-depth analysis. Hence, we track divergences of the momentum-dependent static charge susceptibility, i.e., $1/\chi_c(\boldsymbol{q} = \boldsymbol{Q}_{\rm CO}, \omega = 0) = 0$ that implicate a second order phase transition as function of the electron-doping x and interactions V, U at low temperature $T = 0.005$. We define the leading instability by the divergence of χ_c that occurs at the lowest interaction values $U = U_{cr}(x)$, $V = V_{cr}(x)$ and classify the type of emerging long-range CO by the respective ordering vector $\boldsymbol{Q}_{\rm CO}$. This analysis allows to determine the kind of order immediately beyond the MF phase boundary, but does not allow to map the evolution of the ground state deeper in the emerging phase or associated phase boundaries beyond the critical interactions. To comprehensively discuss the three-dimensional parameter space spanned by U, V and $n = 1 + x$, we first provide phase diagrams in the U-V plane at four fixed densities n in Figs. 1(a)–1(d). These employ extended regions of paramagnetic (PM) and commensurate antiferromagnetic (AFM) ground states that become unstable with respect to additional emerging order at the phase boundaries as indicated. We complement that

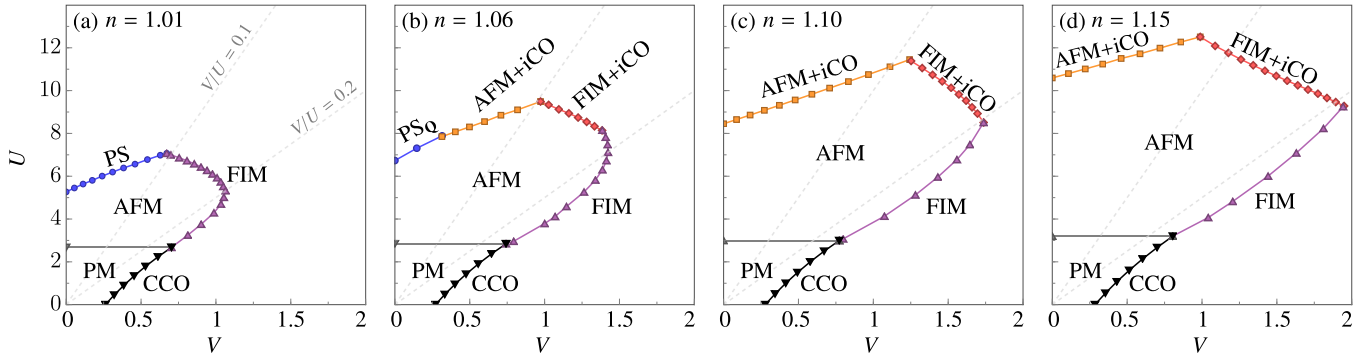

FIG. 1. Phase diagram in the U-V plane at four fixed values of density n as inferred from the stability analysis of the mean-field phases PM and AFM. The emerging charge orders are phase-separated (PS), incommensurate (iCO), or commensurate, i.e., checkerboard charge-order (CCO) or ferrimagnetism (FIM).

illustration by Fig. 2, which shows the emerging phases in the V_{cr}/U_{cr}-n plane, which can be inferred from Fig. 1 at a respectively given filling by moving along the AFM phase boundary for increasing interaction ratios V/U. Additionally, Fig. 2 provides idealized sketches of the corresponding real-space spin and charge configurations within the ordered phases. In total, we detect five distinct types of CO, as we elaborate in the following.

On MF level, the phase boundary between PM to AFM does not depend on the long-range density-density interaction, because magnetic transitions are agnostic to V in that description, compare Eq. (2). For sufficiently high V, however, the PM becomes unstable towards a checkerboard charge order (CCO), implicated by a divergence at $\boldsymbol{Q}_{\rm CO} = (\pi, \pi)$. While the MF ground state becomes AFM, i.e., $\boldsymbol{Q}_{\rm SO} = (\pi, \pi)$ for $U \gtrsim 2.7$, it retains the charge instability at $\boldsymbol{Q}_{\rm CO} = (\pi, \pi)$ for large V, compare Fig. 1. This apparent spin-charge coupling gives rise to an accompanying divergence of the longitudinal static spin susceptibility at the Γ point $1/\chi_s^l(\boldsymbol{q} = 0) = 0$, i.e., the onset of ferrimagnetism (FIM) with two different antiparallel sublattice magnetizations and a net magnetic moment. The emergence of such CCO and FIM is also supported by previous slave-boson MF studies of the extended Hubbard model [53,54].

Small values of V, on the other hand, allow for the formation of PS, implicated by $\boldsymbol{Q}_{\rm CO} = (0, 0)$, which we detect at sufficiently high U and small dopings in full consistency with the previously discussed MF picture. At intermediate doping, the ordering vector evolves to small but finite values [$\boldsymbol{Q}_{\rm CO} = (\epsilon, 0)$, $\epsilon/2\pi \lesssim 0.125$] within a second order transition, whereby the precise value of ϵ depends on U and V. This type of order, labeled PS$_{\boldsymbol{Q}}$, has been discussed in Refs. [29,35,36] and is interpreted as emerging domain walls, driven by the same physical mechanism as PS.

With increasing doping, the kinetic energy gains importance, whereby we detect emerging incommensurate charge order (iCO) with ordering vectors $\boldsymbol{Q}_{\rm iCO} = (Q_{\rm iCO}, 0)$ as modulation of the AFM and $\tilde{\boldsymbol{Q}}_{\rm iCO} = (\pi - Q_{\rm iCO}, \pi)$ of the FIM, respectively. The respective ordering sketches in Fig. 2 are truncated to a finite unit cell, while in general the patterns remain incommensurate in one spatial direction. We identify both types of iCO as a result of Fermi surface instabilities, i.e., kinetic effects due to nesting (intrapocket versus interpocket) within the fermiology of the AFM parent state in the extended zone scheme as illustrated in the insets of Fig. 3. Notably, AFM and FIM ordering tendencies compete at intermediate interaction ratios $V/U \approx 0.1$, resulting in a somewhat enhanced critical interaction scale, compare Fig. 1.

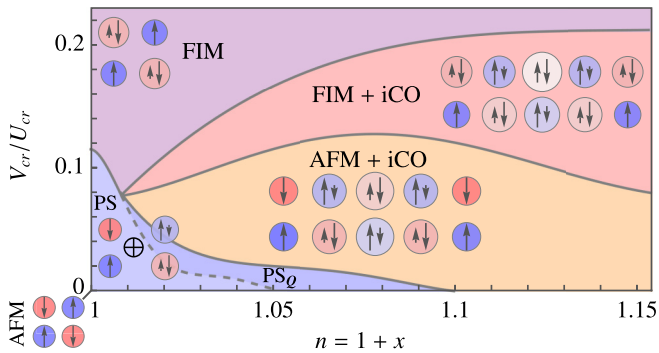

FIG. 2. Phase diagram of emerging CO as a function of electron-doping x and the critical interaction ratio V_{cr}/U_{cr}. Different orders are visualized by idealized sketches, depicting how doped charges arrange in a real-space picture that combines magnetic ($\uparrow, \downarrow$) and charge (circle size) order.

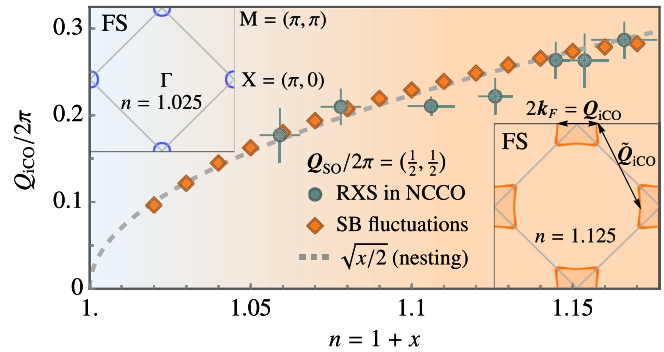

FIG. 3. Incommensurate charge order (iCO) wavevector inferred from SB fluctuations in comparison to RXS data in NCCO adopted from Ref. [9]. Our result for $\boldsymbol{Q}_{\rm iCO}$ follows the diameter of the Fermi surface (FS) that relates to the doping x via Luttinger's theorem (dashed line).

Charge order in NCCO. Emerging iCO that partially overlaps with AFM order has been investigated via resonant x-ray scattering (RXS) experiments by measuring $\boldsymbol{Q}_{\mathrm{iCO}}$ in various electron-doped cuprates [8–12,31]. Among those materials, NCCO employs an extended AFM domain up to dopings of $x \lesssim 0.14$ [55] in agreement with the SB mean-field ground state. Moreover, the FS is presumed to play an important role in determining the iCO wave vector and its doping dependence [8,9,12] but other mechanisms like a momentum-dependent electron-phonon coupling, which is not captured by our model, might also increase the propensity towards CO [53,56]. Figure 3 shows Q_{iCO} inferred from the SB fluctuation calculation and RXS measurements in NCCO, demonstrating rather good agreement. Within our theory, we can clearly establish the association $Q_{\mathrm{iCO}} = 2k_F$ between the iCO wave vector and the FS, which implies the iCO to be nesting-enhanced. In contrast to the original Peierls argument, in our case a diverging bare susceptibility $\chi_0(Q, 0)$ at $Q = 2k_{\mathrm{F}}$ is not necessary to drive the charge instability. It is sufficient to have an enhancement of $\chi_0(2k_{\mathrm{F}}, 0)$, because of the available considerable interaction strength. According to Luttinger's theorem the enclosed area of the FS is equal to the doping x, whereby we estimate $2k_{\mathrm{F}}/2\pi \approx \sqrt{x/2}$ under the approximation of square-shaped FSs, which appears to match the observed iCO wave vector quite well.

The emerging CO begins to show up already below the critical interaction U_{cr} in the form of short-range correlations, as implied by a finite peak of χ_c at the same wavevector $\boldsymbol{Q}_{\mathrm{iCO}}$, turning out to be almost independent of the interactions U, V [33]. Indeed, the correlation length ξ extracted from RXS measurements in NCCO is estimated to be rather short ranged with $\xi \approx 5$ unit cells [9,12]. Furthermore, it has been shown that the CO correlations at $\boldsymbol{Q}_{\mathrm{iCO}}$ in the AFM + iCO phase remain visible at elevated temperatures beyond the AFM Néel temperature for sufficiently high dopings $x \gtrsim 0.08$ [9]. In line with this, these short-range correlations are also present within the PM domain of our theory, where χ_c employs a finite nesting peak at $\boldsymbol{Q}_{\mathrm{iCO}}$. Back-folding of the FS at the transition from PM to AFM order enhances this type of nesting for electron doping. For hole doping, the situation is fundamentally different. While there is a nesting peak on the Γ-X high symmetry line similar to electron doping within the PM ground state, that type of nesting is completely removed within the AFM as shown in the SM [33].

Finally, we discuss dynamic excitations and the integrated structure factors

$$S_{c,s}(\boldsymbol{q}) = 1/\pi \int_{\Omega_{\mathrm{min}}}^{\Omega_{\mathrm{max}}} d\omega \, \mathrm{Im}\, \chi_{c,s}(\boldsymbol{q}, \omega)[1 + n_{\mathrm{B}}(\omega)], \qquad (4)$$

with $n_{\mathrm{B}}(\omega) = 1/(\mathrm{e}^{\omega/T} - 1)$, which can directly be related to resonant inelastic x-ray scattering (RIXS) [57]. Thereby, da Silva Neto *et al.* revealed that roughly half of the signal at $\boldsymbol{Q}_{\mathrm{iCO}}$ can be attributed to the quasielastic line, i.e., $\omega = 0$, which supports the claim of static CO. Additional high-energy dynamic contributions near $\boldsymbol{Q}_{\mathrm{iCO}}$, appear mainly in the crossed-polarized channel, i.e., are indicated to be magnetic in nature and follow the paramagnon dispersion [11].

Within our theory, we detect (para-)magnons in the transversal spin channel χ_s^t. At low dopings, we find their dispersion to be sharp and to match linear spin-wave theory [33], which is the signature of magnons and is in quantitative agreement with RIXS measurements in NCCO [30]. With increasing doping we observe a broadening of the mode, which reflects the reduced correlation length and lifetime of paramagnons. Moreover, as shown in Fig. 4 for $x = 0.147$, we find the paramagnon dispersion, in agreement with experimental evidence [30], to deviate from linear spin-wave theory, which is displayed by the dashed line. Notably, we determine a nesting-enhanced, noncollective mode around $\boldsymbol{Q}_{\mathrm{iCO}}$ that merges with the paramagnon branch at $E \approx 400$ meV, where the experimentally measured high-energy contributions to $\boldsymbol{Q}_{\mathrm{iCO}}$ are centered for that doping. The respective RIXS data [11] suggest that this effect may also be present in NCCO, but polarimetric measurements with higher energy resolution are needed for confirmation.

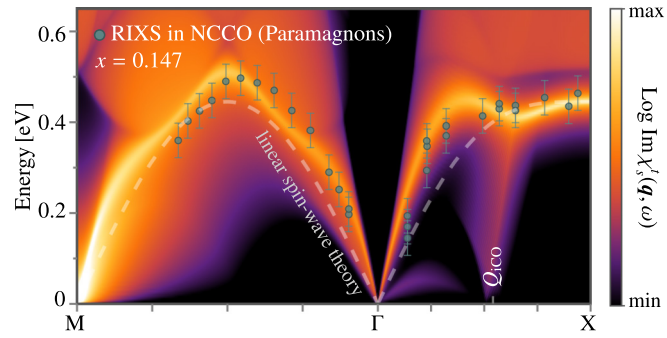

FIG. 4. Paramagnon dispersion on the high-symmetry path, which appears as bright line in the color-coded plot of $\mathrm{Im}\chi_s^t(\boldsymbol{q}, \omega)$ at $(U, V) = (5.5, 0.55)$, along with RIXS data in NCCO (circles with error bars) adopted from Ref. [30]. The absolute energy scale in our model is fitted to $t = 0.52$ eV. The dashed line displays linear spin-wave theory with the velocity $c_s = 1.24$ eVÅ adopted from Ref. [30].

Besides, RIXS experiments revealed a gapped collective mode around the Γ point [30] that has been identified as charge mode and is also present in $La_{2-x}Ce_xCuO_4$ (LCCO) [31]. In qualitative agreement, we detect such a mode in the charge channel but the gap size does not match quantitatively, compare SM [33]. This discrepancy could be due to a three-dimensional nature of the charge mode. Measurements revealed the gap size to depend on the out-of-plane momentum q_z, whereas the paramagnons did not disperse appreciably along q_z [31].

In contrast to χ_s^t, the charge χ_c and longitudinal χ_s^l spin-channel feature significant spectral weight at $\boldsymbol{Q}_{\mathrm{iCO}}$ for $\omega = 0$. However, a direct measurement of the elastic line is subtle because soft x-ray RIXS is done in a reflection-scattering geometry, which leads to an increased signal for small momenta. Therefore, we compare our results for the respective structure factors at doping $x = 0.108$ in Fig. 5 with RIXS data that includes small energies but not strictly the elastic line. The signal shown in the inset contains contributions from the charge and spin channel with integrated energies $E \in (60, 900)$ meV and $\Delta E \approx 60$ meV [11]. If we gauge our energy scale with *ab initio* calculations in NCCO, i.e., $t \approx 0.42$ eV [22], the temperatures shown in the theoretical and experimental data are comparable. Notably, Ref. [11] also revealed a coupling between dynamic magnetic and charge

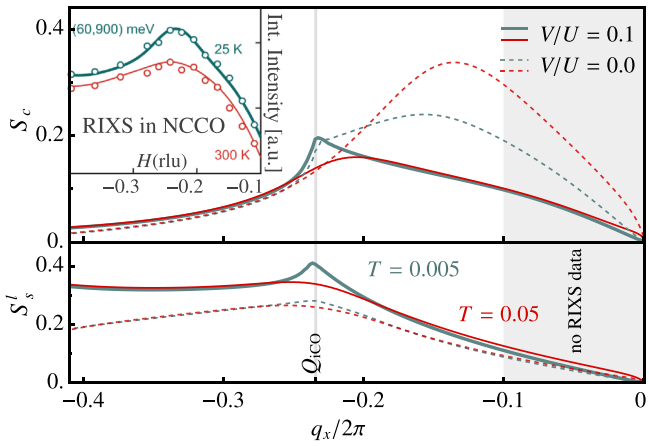

FIG. 5. Charge (S_c) and longitudinal (S^l_s) spin-structure factor for $x = 0.108$ and $(U, V) \approx (U_{cr}, V_{cr})$, i.e., (8.7,0) and (11.5,1.15) as function of $\boldsymbol{q} = (q_x, 0)$ for the energy cutoffs $\Omega_{\min} = 0.01$, $\Omega_{\max} = 2$. The inset shows RIXS data in NCCO adopted from Ref. [11] with the same doping and comparable energy cutoffs.

correlations in line with our theoretical predictions. As a result, S_c and S^l_s feature a coinciding peak at $\boldsymbol{Q}_{\rm iCO}$ that significantly flattens at room temperature like the RIXS signal. This qualitative agreement, however, requires a finite NN interaction V that reduces the spectral weight in the charge channel at low momenta and enhances the signal at $\boldsymbol{Q}_{\rm iCO}$ in the longitudinal spin channel. For $V = 0$, we predict a second excitation peak in S_c due to the propensity towards phase separation ($\mathrm{PS}_{\boldsymbol{Q}}$), which is not supported by the available experimental data. According to *ab initio* calculations in the cuprates [58] even longer-ranged interactions might be non-negligible and would extend the experimentally observed AFM + iCO state by further suppressing PS and weakening FIM ordering tendencies.

Conclusion. We identify the electron-doped extended Hubbard model, including a nonlocal interaction V, to feature nesting-enhanced incommensurate charge order on top of a commensurate AFM background. Equipped with dynamical correlation profiles received from our slave-boson fluctuation analysis, we achieve quantitative correspondence with experimental evidence from resonant inelastic x-ray scattering in NCCO, including the doping dependence of the CO wave vector $\boldsymbol{Q}_{\rm iCO}$. Our study resolves the intricacy of intertwined spin and charge order in cuprates, and highlights the use of slave-boson theories for multiorder phenomena in correlated electron systems.

Acknowledgments. The authors thank Werner Hanke, Masa Imada, and Giorgio Sangiovanni for helpful discussions. The work in Würzburg is funded by Deutsche Forschungsgemeinschaft (DFG, German Research Foundation), Project No. 258499086 - SFB 1170 and the Würzburg-Dresden Cluster of Excellence on Complexity and Topology in Quantum Matter *ct.qmat* Project No. 390858490 - EXC 2147. Peter Wölfle acknowledges support through a Distinguished Senior Fellowship of Karlsruhe Institute of Technology. Eduardo H. da Silva Neto acknowledges support by the Alfred P. Sloan Fellowship and the National Science Foundation, Grant No. DMR-2034345.

[1] J. M. Tranquada, B. J. Sternlieb, J. D. Axe, Y. Nakamura, and S. Uchida, Nature (London) **375**, 561 (1995).
[2] N. P. Armitage, P. Fournier, and R. L. Greene, Rev. Mod. Phys. **82**, 2421 (2010).
[3] G. Ghiringhelli, M. L. Tacon, M. Minola, S. Blanco-Canosa, C. Mazzoli, N. B. Brookes, G. M. D. Luca, A. Frano, D. G. Hawthorn, F. He, T. Loew, M. M. Sala, D. C. Peets, M. Salluzzo, E. Schierle, R. Sutarto, G. A. Sawatzky, E. Weschke, B. Keimer, and L. Braicovich, Science **337**, 821 (2012).
[4] J. Chang, E. Blackburn, A. T. Holmes, N. B. Christensen, J. Larsen, J. Mesot, R. Liang, D. A. Bonn, W. N. Hardy, A. Watenphul, M. v. Zimmermann, E. M. Forgan, and S. M. Hayden, Nat. Phys. **8**, 871 (2012).
[5] W. Tabis, Y. Li, M. L. Tacon, L. Braicovich, A. Kreyssig, M. Minola, G. Dellea, E. Weschke, M. J. Veit, M. Ramazanoglu, A. I. Goldman, T. Schmitt, G. Ghiringhelli, N. Barišić, M. K. Chan, C. J. Dorow, G. Yu, X. Zhao, B. Keimer, and M. Greven, Nat. Commun. **5**, 5875 (2014).
[6] R. Comin, A. Frano, M. M. Yee, Y. Yoshida, H. Eisaki, E. Schierle, E. Weschke, R. Sutarto, F. He, A. Soumyanarayanan, Y. He, M. L. Tacon, I. S. Elfimov, J. E. Hoffman, G. A. Sawatzky, B. Keimer, and A. Damascelli, Science **343**, 390 (2014).
[7] E. H. da Silva Neto, P. Aynajian, A. Frano, R. Comin, E. Schierle, E. Weschke, A. Gyenis, J. Wen, J. Schneeloch, Z. Xu, S. Ono, G. Gu, M. L. Tacon, and A. Yazdani, Science **343**, 393 (2014).
[8] E. H. Da Silva Neto, R. Comin, F. He, R. Sutarto, Y. Jiang, R. L. Greene, G. A. Sawatzky, and A. Damascelli, Science **347**, 282 (2015).
[9] E. H. da Silva Neto, B. Yu, M. Minola, R. Sutarto, E. Schierle, F. Boschini, M. Zonno, M. Bluschke, J. Higgins, Y. Li, G. Yu, E. Weschke, F. He, M. L. Tacon, R. L. Greene, M. Greven, G. A. Sawatzky, B. Keimer, and A. Damascelli, Sci. Adv. **2**, e1600782 (2016).
[10] R. Comin and A. Damascelli, Annu. Rev. Condens. Matter Phys. **7**, 369 (2016).
[11] E. H. da Silva Neto, M. Minola, B. Yu, W. Tabis, M. Bluschke, D. Unruh, H. Suzuki, Y. Li, G. Yu, D. Betto, K. Kummer, F. Yakhou, N. B. Brookes, M. Le Tacon, M. Greven, B. Keimer, and A. Damascelli, Phys. Rev. B **98**, 161114(R) (2018).
[12] M. Kang, J. Pelliciari, A. Frano, N. Breznay, E. Schierle, E. Weschke, R. Sutarto, F. He, P. Shafer, E. Arenholz, M. Chen, K. Zhang, A. Ruiz, Z. Hao, S. Lewin, J. Analytis, Y. Krockenberger, H. Yamamoto, T. Das, and R. Comin, Nat. Phys. **15**, 335 (2019).
[13] R. Arpaia, S. Caprara, R. Fumagalli, G. D. Vecchi, Y. Y. Peng, E. Andersson, D. Betto, G. M. D. Luca, N. B. Brookes, F. Lombardi, M. Salluzzo, L. Braicovich, C. D. Castro, M. Grilli, and G. Ghiringhelli, Science **365**, 906 (2019).
[14] R. Arpaia and G. Ghiringhelli, J. Phys. Soc. Jpn. **90**, 111005 (2021).
[15] S. Wandel, F. Boschini, E. H. da Silva Neto, L. Shen, M. X. Na, S. Zohar, Y. Wang, S. B. Welch, M. H. Seaberg, J. D.

Koralek, G. L. Dakovski, W. Hettel, M.-F. Lin, S. P. Moeller, W. F. Schlotter, A. H. Reid, M. P. Minitti, T. Boyle, F. He, R. Sutarto *et al.*, Science **376**, 860 (2022).
[16] E. Fradkin, S. A. Kivelson, and J. M. Tranquada, Rev. Mod. Phys. **87**, 457 (2015).
[17] K. Yamada, C. H. Lee, K. Kurahashi, J. Wada, S. Wakimoto, S. Ueki, H. Kimura, Y. Endoh, S. Hosoya, G. Shirane, R. J. Birgeneau, M. Greven, M. A. Kastner, and Y. J. Kim, Phys. Rev. B **57**, 6165 (1998).
[18] S. A. Kivelson, I. P. Bindloss, E. Fradkin, V. Oganesyan, J. M. Tranquada, A. Kapitulnik, and C. Howald, Rev. Mod. Phys. **75**, 1201 (2003).
[19] A. Macridin, M. Jarrell, T. Maier, and G. A. Sawatzky, Phys. Rev. B **71**, 134527 (2005).
[20] T. Das, R. Markiewicz, and A. Bansil, Adv. Phys. **63**, 151 (2014).
[21] M. Hirayama, Y. Yamaji, T. Misawa, and M. Imada, Phys. Rev. B **98**, 134501 (2018).
[22] R. S. Markiewicz, S. Sahrakorpi, M. Lindroos, H. Lin, and A. Bansil, Phys. Rev. B **72**, 054519 (2005).
[23] M. Hirayama, T. Misawa, T. Ohgoe, Y. Yamaji, and M. Imada, Phys. Rev. B **99**, 245155 (2019).
[24] F. Boschini, M. Minola, R. Sutarto, E. Schierle, M. Bluschke, S. Das, Y. Yang, M. Michiardi, Y. C. Shao, X. Feng, S. Ono, R. D. Zhong, J. A. Schneeloch, G. D. Gu, E. Weschke, F. He, Y. D. Chuang, B. Keimer, A. Damascelli, A. Frano *et al.*, Nat. Commun. **12**, 597 (2021).
[25] M. Bejas, R. Zeyher, and A. Greco, Phys. Rev. B **106**, 224512 (2022).
[26] K. Scott, E. Kisiel, T. J. Boyle, R. Basak, G. Jargot, S. Das, S. Agrestini, M. Garcia-Fernandez, J. Choi, J. Pelliciari, J. Li, Y. D. Chuang, R. D. Zhong, J. A. Schneeloch, G. D. Gu, F. Légaré, A. F. Kemper, K.-J. Zhou, V. Bisogni, S. Blanco-Canosa *et al.*, Sci. Adv. **9**, eadg3710 (2023).
[27] J. P. F. LeBlanc, A. E. Antipov, F. Becca, I. W. Bulik, G.-L. Chan, C.-M. Chung, Y. Deng, M. Ferrero, T. M. Henderson, C. A. Jiménez-Hoyos, E. Kozik, X.-W. Liu, A. J. Millis, N. V. Prokof'ev, M. Qin, G. E. Scuseria, H. Shi, B. V. Svistunov, L. F. Tocchio, I. S. Tupitsyn *et al.*, Phys. Rev. X **5**, 041041 (2015).
[28] G. Kotliar and A. E. Ruckenstein, Phys. Rev. Lett. **57**, 1362 (1986).
[29] J. Seufert, D. Riegler, M. Klett, R. Thomale, and P. Wölfle, Phys. Rev. B **103**, 165117 (2021).
[30] W. S. Lee, J. J. Lee, E. A. Nowadnick, S. Gerber, W. Tabis, S. W. Huang, V. N. Strocov, E. M. Motoyama, G. Yu, B. Moritz, H. Y. Huang, R. P. Wang, Y. B. Huang, W. B. Wu, C. T. Chen, D. J. Huang, M. Greven, T. Schmitt, Z. X. Shen, and T. P. Devereaux, Nat. Phys. **10**, 883 (2014).
[31] M. Hepting, L. Chaix, E. W. Huang, R. Fumagalli, Y. Y. Peng, B. Moritz, K. Kummer, N. B. Brookes, W. C. Lee, M. Hashimoto, T. Sarkar, J. F. He, C. R. Rotundu, Y. S. Lee, R. L. Greene, L. Braicovich, G. Ghiringhelli, Z. X. Shen, T. P. Devereaux, and W. S. Lee, Nature (London) **563**, 374 (2018).
[32] R. Frésard and P. Wölfle, Int. J. Mod. Phys. B **06**, 685 (1992).
[33] See Supplemental Material at http://link.aps.org/supplemental/10.1103/PhysRevB.108.195141 for a recap of the established slave-boson formalism along with a derivation of the newly implemented long-range interaction V within the slave-boson meanfield and fluctuation theory. Moreover, we elaborate on the numerical data analysis and provide additional background information in the context of phase separation and collective modes.
[34] D. Riegler, M. Klett, T. Neupert, R. Thomale, and P. Wölfle, Phys. Rev. B **101**, 235137 (2020).
[35] D. Riegler, Ph.D. thesis, Emergent phenomena in strongly correlated electron systems: Auxiliary particle approach to the many-body problem, University of Wuerzburg, Wuerzburg, Germany, 2022.
[36] M. Klett, Ph.D. thesis, Auxiliary particle approach for strongly correlated electrons: How interaction shapes order, University of Wuerzburg, Wuerzburg, Germany, 2021.
[37] T. Li, Y. S. Sun, and P. Wölfle, Z. Phys. B: Condens. Matter **82**, 369 (1991).
[38] W. Zimmermann, R. Frésard, and P. Wölfle, Phys. Rev. B **56**, 10097 (1997).
[39] R. Frésard and P. Wölfle, J. Phys.: Condens. Matter **4**, 3625 (1992).
[40] P. A. Igoshev, M. A. Timirgazin, V. F. Gilmutdinov, A. K. Arzhnikov, and V. Y. Irkhin, J. Phys.: Condens. Matter **27**, 446002 (2015).
[41] B.-X. Zheng and G. K.-L. Chan, Phys. Rev. B **93**, 035126 (2016).
[42] E. W. Huang, C. B. Mendl, H.-C. Jiang, B. Moritz, and T. P. Devereaux, npj Quant Mater **3**, 22 (2019).
[43] M. Klett, J. Beyer, D. Riegler, J. Seufert, P. Wölfle, S. Rachel, and R. Thomale (unpublished).
[44] J. Wen, Z. Xu, G. Xu, J. M. Tranquada, G. Gu, S. Chang, and H. J. Kang, Phys. Rev. B **78**, 212506 (2008).
[45] S. Lee, E. W. Huang, T. A. Johnson, X. Guo, A. A. Husain, M. Mitrano, K. Lu, A. V. Zakrzewski, G. A. de la Peña, Y. Peng, H. Huang, S.-J. Lee, H. Jang, J.-S. Lee, Y. I. Joe, W. B. Doriese, P. Szypryt, D. S. Swetz, S. Chi, A. A. Aczel *et al.*, Proc. Natl. Acad. Sci. USA **119**, e2119429119 (2022).
[46] P. A. Igoshev, M. A. Timirgazin, A. A. Katanin, A. K. Arzhnikov, and V. Y. Irkhin, Phys. Rev. B **81**, 094407 (2010).
[47] M. Crispino, M. Chatzieleftheriou, T. Gorni, and L. de' Medici, Phys. Rev. B **107**, 155149 (2023).
[48] M. Raczkowski, R. Frésard, and A. M. Oleś, Phys. Rev. B **73**, 174525 (2006).
[49] A. Damascelli, Z. Hussain, and Z.-X. Shen, Rev. Mod. Phys. **75**, 473 (2003).
[50] E. Liarokapis, Condensed Matter **4**, 87 (2019).
[51] S. Julià-Farré, A. Dauphin, R. W. Chhajlany, P. T. Grochowski, S. Wall, M. Lewenstein, and P. R. Grzybowski, Phys. Rev. B **101**, 125107 (2020).
[52] N. Harima, J. Matsuno, A. Fujimori, Y. Onose, Y. Taguchi, and Y. Tokura, Phys. Rev. B **64**, 220507(R) (2001).
[53] M. Deeg, H. Fehske, and H. Büttner, Z. Phys. B **91**, 31 (1993).
[54] L. Philoxene, V. H. Dao, and R. Frésard, Phys. Rev. B **106**, 235131 (2022).
[55] E. Motoyama, G. Yu, I. Vishik, O. Vajk, P. Mang, and M. Greven, Nature (London) **445**, 186 (2007).
[56] M. D. Johannes and I. I. Mazin, Phys. Rev. B **77**, 165135 (2008).
[57] L. J. P. Ament, M. van Veenendaal, T. P. Devereaux, J. P. Hill, and J. van den Brink, Rev. Mod. Phys. **83**, 705 (2011).
[58] J.-B. Morée, M. Hirayama, M. T. Schmid, Y. Yamaji, and M. Imada, Phys. Rev. B **106**, 235150 (2022).